Supplementary Information

Novel Platinum(II) Compounds with *O,S* Bidentate Ligands: Synthesis, Characterization, Antiproliferative Properties and Biomolecular Interactions

Carolin Mügge, Ruiqi Liu, Helmar Görls, Chiara Gabbiani, Elena Michelucci, Nadine Rüdiger, Joachim H. Clement, Luigi Messori,* Wolfgang Weigand*

Table of contents

Additional Syntheses

4-Bromo-β-hydroxy dithiocinnamic ethyl ester (2)

Using 4-bromo-acetophenone (2 g, 10.05 mmol), KO^{t}Bu (2.26 g, 20.1 mmol), CS_2 (0.85 mL, 10.05 mmol), and ethyl iodide (0.81 mL, 10.05 mmol), synthesis was carried out according to general procedure 1. Column chromatography was accomplished with hexane/dichloromethane 1:1 as mobile phase ($R_f \approx 0.6$) and yielded **2** (2.185 g, 72 %) as orange solid.

M.p. 69 °C;
^{1}H NMR (200 MHz, $CDCl_3$, 25°C, TMS): δ = 2.65 (t, 3H, CH_3), 3.26 (q, 2H, SCH_2), 6.83 (s, 1H, C*H*CS_2), 7.65 (d, $^3J_{H2\text{-}H3}$ = 8.8 Hz, 2H, Ar-H2), 7.72 (d, $^3J_{H2\text{-}H3}$ = 8.8 Hz, 2H, Ar-H3), 15.06 (s, 1H, OH);
^{13}C{^{1}H} NMR (50 MHz, $CDCl_3$, 25°C, TMS): δ = 12.8 (CH_3), 28.0 (SCH_2), 107.7 (*C*HCS_2), 126.4 (Ar-C4), 128.1 (Ar-C2), 132.0 (Ar-C3), 133.3 (Ar-C1), 168.2 (COH), 216.9 (CS_2);
FTIR (KBr): $\tilde{\nu}$ = 3400, 3059, 2975, 2932, 2922, 1591, 1561, 1484, 1421, 1413, 1252, 1236, 1075 (s), 1061, 1007, 964, 949, 833, 790, 763 cm^{-1};
MS (DEI): *m/z* = 304 $[M+2]^+$, 302 $[M]^+$, 243 $[M\text{-}SEt+H]^+$, 241, 185, 183, 162, 105, 85, 77;
elemental analysis calcd for $C_{11}H_{11}BrOS_2$: C 43.57, H 3.66, S 21.15, Br 26.35 %; **found:** C 43.70, H 3.51, S 21.16, Br 26.68 %.

β-Hydroxy dithiocinnamic ethyl ester (5)

Following general procedure 1, acetophenone (2 g, 16.65 mmol), KO^{t}Bu (3.74 g, 33.3 mmol), CS_2 (1.4 mL, 23.31 mmol), and ethyl iodide (1.35 mL, 16.65 mmol) were brought to reaction. Column chromatography was achieved with hexane/dichloromethane 1:1 as mobile phase ($R_f \approx 0.7$) and afforded 2.41 g (64 %) of **5** as green-yellow oil.

^{1}H NMR (200 MHz, $CDCl_3$, 25°C, TMS): δ = 1.52 (t, 3H, CH_3), 3.24 (q, 2H, SCH_2), 6.88 (s, 1H, C*H*CS_2), 7.37-7.49 (m, 3H, Ar-H3,4), 7.82-7-89 (m, 2H, Ar-H2), 15.11 (s, 1H, OH);
^{13}C{^{1}H} NMR (50 MHz, $CDCl_3$, 25°C, TMS): δ = 12.9 (CH_3), 27.8 (SCH_2), 107.8 (*C*HCS_2), 126.6 (Ar-C2), 128.7 (Ar-C3), 131.8 (Ar-C4), 134.3 (Ar-C1), 169.6 (COH), 216.6 (CS_2);
FTIR (KBr): $\tilde{\nu}$ = 3061, 2969, 2926, 2870, 1589, 1560, 1493, 1452, 1397, 1265, 1232, 1063, 949, 827, 762 cm^{-1};
MS (DEI): *m/z* = 224 $[M]^+$, 196 $[M\text{-}Et+H]^+$, 163 $[M\text{-}SEt+H]^+$, 105, 85, 77;
elemental analysis calcd for $C_{11}H_{12}OS_2$: C 58.89, H 5.39, S 28.59 %, **found:** C 58.69 H 5.57, S 28.66 %

β-Hydroxy dithiocinnamic hexyl ester (6)

Synthesis was carried out according to general procedure 1 with acetophenone (2 g, 16.65 mmol), KO^{t}Bu (3.74 g, 33.3 mmol), CS2 (1.4 mL, 23.31 mmol), and hexyl bromide (2.33 mL, 16.65 mmol) as reagents. Purification via column chromatography with hexane/dichloromethane 1:1 as eluent ($R_f \approx 0.7$) afforded the pure product (1.05 g, 22 %) as yellow oil.

^{1}H NMR (200 MHz, $CDCl_3$, 25°C, TMS): δ = 0.86-0.92 (m, 3H, CH_3), 1.27-1.52 (m, 6H, 3x CH_2), 1.64-1.79 (m, 2H, SCH_2CH_2), 3.25 (t, 2H, SCH_2), 6.90 (s, 1H, $CHCS_2$), 7.37-7.53 (m, 3H, Ar-H3,4), 7.83-7-88 (m, 2H, Ar-H2), 15.12 (s, 1H, OH);
^{13}C{^{1}H} NMR (50 MHz, $CDCl_3$, 25°C, TMS): δ = 13.9 (CH_3), 22.5 (CH_2CH_3), 27.8 ($CH_2CH_2CH_3$), 28.7 ($SCH_2CH_2CH_2$), 31.3 (SCH_2CH_2), 33.6 (SCH_2), 107.9 ($CHCS_2$), 126.6 (Ar-C2), 128.7 (Ar-C3), 131.8 (Ar-C4), 134.3 (Ar-C1), 169.4 (COH), 216.7 (CS_2);
FTIR (KBr): $\tilde{\nu}$ = 3300, 3062, 2956, 2928, 2856, 1589, 1561, 1492, 1453, 1252, 1232, 1056, 949, 828, 763 cm^{-1};
MS (DEI): *m/z* = 280 $[M]^+$, 196 $[M\text{-}Hex+H]^+$, 163, 105, 85, 77;
elemental analysis calcd for $C_{15}H_{20}OS_2$: for $C_{15}H_{20}OS_2 \cdot 0.4\, C_6H_{14}$: C 66.36, H 8.19, S 20.36 %; **found:** C 66.32, H 8.06, S 20.38 %.

Bis(1-phenyl-3-(methylthio)-3-thioxo-prop-1-en-1-olate-*O,S*)-platinum(II) (13)

As a side product to the synthesis of **10**, the bischelate **13** was isolated ($R_f \approx 0.7$, 10 mg as bright red solid). Single crystals were obtained by slow evaporation of hexane.

^{1}H NMR (200 MHz, $CDCl_3$): δ = 2.63 (s, 6H, CH_3), 7.12 (s, 2H, C*H*CS_2), 7.39-7.60 (m, 6H, Ar-H3,4), 7.99-8.04 (m, 4H, Ar-H2) ppm.
^{13}C{^{1}H} NMR (50 MHz, $CDCl_3$): δ = 17.6 (CH_3), 112.5 (*C*HCS_2), 127.3 (Ar-C2), 128.8 (Ar-C3), 131.3 (Ar-C4), 138.9 (Ar-C1), 174.2 (CO), 177.8 (CS_2) ppm.
MS (DEI): *m/z* =613 $[M]^+$.

Bis(1-phenyl-3-(hexylthio)-3-thioxo-prop-1-en-1-olate-*O,S*)-platinum(II) (14)

As a side product to the synthesis of **12**, the bischelate **14** was isolated ($R_f \approx 0.7$, 30 mg bright red solid). Single crystals were obtained by slow evaporation of hexane.

^{1}H NMR (200 MHz, $CDCl_3$): δ = 0.82-0.91 (m, 6H, CH_3), 1.23-1.50 (m, 12H, 3x CH_2), 1.76 (qui, 4H, SCH_2CH_2), 3.18 (t, 4H, SCH_2), 7.07 (s, 2H, C*H*CS_2), 7.36-7.56 (m, 6H, Ar-H3,4), 7.96-8.00 (m, 4H, Ar-H2) ppm.
^{13}C{^{1}H} NMR (50 MHz, $CDCl_3$): δ = 14.0 (CH_3), 22.5 (CH_2CH_3), 28.2 ($CH_2CH_2CH_3$), 28.6 ($SCH_2CH_2CH_2$), 31.3 (SCH_2CH_2), 34.3 (SCH_2), 112.7 (*C*HCS_2), 127.3 (Ar-C2), 128.7 (Ar-C3), 131.2 (Ar-C4), 139.1 (Ar-C1), 174.2 (CO), 177.3 (CS_2) ppm.
MS (DEI): *m/z* = 754 $[M]^+$.

Crystallographic data

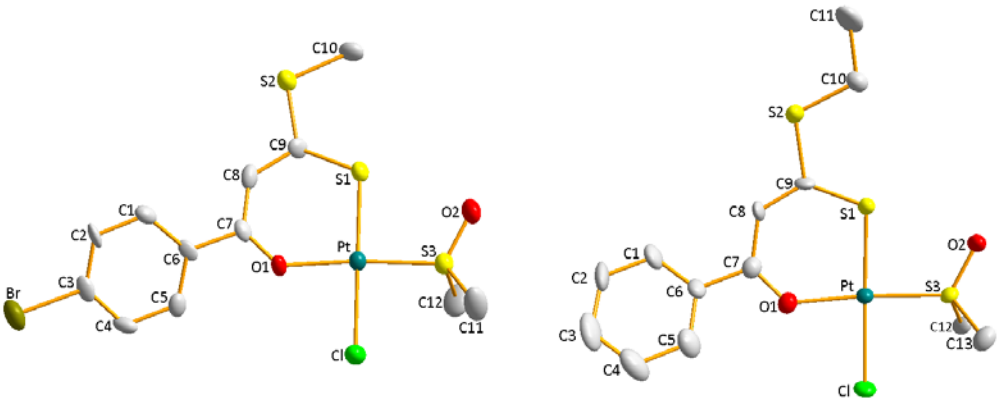

Figure S1. Molecular structures of **7** (left) and **11** (right). Thermal ellipsoids are given at the 50 % propability level.

Table S1. Selected bond lengths and angles for the crystal structures of **7** and **11**.

Bond lengths [Å]			
7		**11**	
Pt-O1	2.013(5)	Pt-O1	2.006(5)
Pt-S1	2.253(2)	Pt-S1	2.249(2)
Pt-S3	2.200(2)	Pt-S3	2.186(2)
Pt-Cl	2.336(2)	Pt-Cl	2.3597(19)
O1-C7	1.251(9)	O1-C7	1.285(9)
C7-C8	1.403(11)	C7-C8	1.426(11)
C8-C9	1.425(11)	C8-C9	1.366(10)
S1-C9	1.668(9)	S1-C9	1.674(8)
S3-O2	1.457(6)	S3-O2	1.472(6)
S3-C11	1.754(8)	S3-C12	1.772(8)
S3-C12	1.761(9)	S3-C13	1.770(7)

Bond angles [°]			
7		**11**	
O1-Pt-S1	96.11(17)	O1-Pt-S1	96.02(16)
S1-Pt-S3	88.32(8)	S1-Pt-S3	88.50(7)
S3-Pt-Cl	91.33(9)	S3-Pt-Cl	90.20(7)
O1-Pt-Cl	84.21(17)	O1-Pt-Cl	85.28(16)
S1-Pt-Cl	177.94(9)	S1-Pt-Cl	178.47(7)
O1-Pt-S3	175.49(17)	O1-Pt-S3	175.39(16)
Pt-O1-C7	130.9(6)	Pt-O1-C7	130.5(5)
O1-C7-C8	127.1(8)	O1-C7-C8	126.7(7)
C7-C8-C9	128.0(8)	C7-C8-C9	127.3(8)
C8-C9-S1	128.7(7)	C8-C9-S1	130.8(6)
C9-S1-Pt	108.6(3)	C9-S1-Pt	108.6(3)
O2-S3-C11	107.9(4)	O2-S3-C12	107.7(4)
O2-S3-C12	108.5(4)	O2-S3-C13	107.8(4)
C11-S3-C12	101.8(5)	C12-S3-C13	102.3(4)
O2-S3-Pt	117.0(3)	O2-S3-Pt	118.7(2)
C11-S3-Pt	111.6(3)	C12-S3-Pt	108.5(3)
C12-S3-Pt	108.9(3)	C13-S3-Pt	110.5(3)

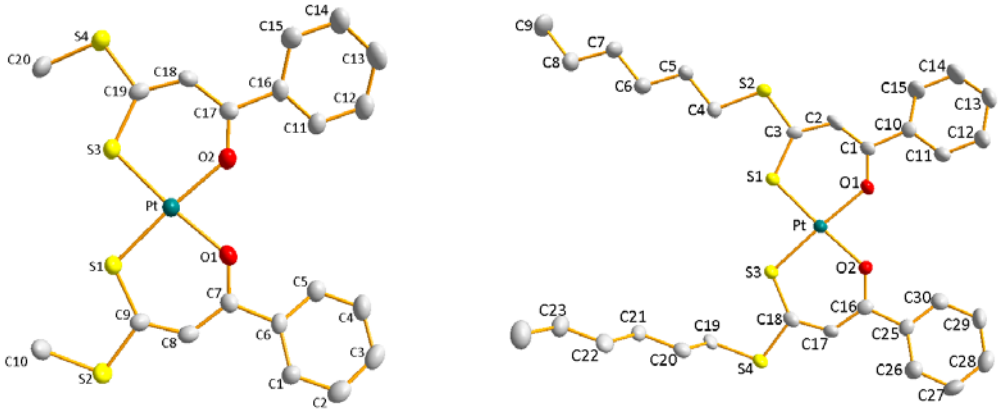

Figure S2. Crystal structures of **13** (left) and **14** (right). Thermal ellipsoids are given at the 50 % propability level.

Table S2. Selected bond lengths and angles for **13** and **14**.

Bond lengths [Å]			
13		**14**	
Pt-O1	2.018(4)	Pt-O1	2.028(3)
Pt-S1	2.2333(18)	Pt-S1	2.2252(12)
Pt-O2	2.007(5)	Pt-O2	2.013(3)
Pt-S3	2.2323(17)	Pt-S3	2.2306(12)
O1-C7	1.273(8)	O1-C1	1.279(5)
C7-C8	1.397(9)	C1-C2	1.389(6)
C8-C9	1.382(9)	C2-C3	1.382(6)
S1-C9	1.701(7)	S1-C3	1.702(4)
O2-C17	1.270(8)	O2-C16	1.281(5)
C17-C18	1.404(9)	C16-C17	1.393(6)
C18-C19	1.384(9)	C17-C18	1.388(6)
S3-C19	1.696(7)	S3-C18	1.690(5)

Bond angles [°]			
13		**14**	
O1-Pt-S1	96.31(15)	O1-Pt-S1	96.72(9)
S1-Pt-S3	87.98(6)	S1-Pt-S3	86.06(4)
O2-Pt-S3	96.03(13)	O2-Pt-S3	96.73(9)
O1-Pt-O2	79.65(19)	O1-Pt-O2	80.54(12)
O1-Pt-S3	175.29(14)	O1-Pt-S3	176.89(9)
O2-Pt-S1	175.85(13)	O2-Pt-S1	176.75(9)
Pt-O1-C7	130.8(4)	Pt-O1-C1	129.5(3)
O1-C7-C8	126.1(6)	O1-C1-C2	127.2(4)
C7-C8-C9	129.4(7)	C1-C2-C3	128.8(4)
C8-C9-S1	128.7(6)	C2-C3-S1	129.2(4)
C9-S1-Pt	108.6(2)	C3-S1-Pt	108.43(16)
Pt-O2-C17	132.0(4)	Pt-O2-C16	130.8(3)
O2-C17-C18	125.4(6)	O2-C16-C17	125.0(4)
C17-C18-C19	128.4(7)	C16-C17-C18	130.3(5)
C18-C19-S3	129.7(5)	C17-C18-S3	128.6(4)
C19-S3-Pt	108.2(2)	C18-S3-Pt	108.38(16)

^{1}H and ^{13}C{^{1}H} NMR spectra of bischelates **13** and **14** are almost identical to those of the corresponding monochelated species, with the only difference being non-existent DMSO signals.

For the bischelates **13** and **14**, X-ray quality crystals were obtained as well. They are depicted in Figure S2, selected bond lengths and angles are given in Table S1. The two ligands are *cis* coordinated, as reported for analogous structures earlier[1]. The *cis* coordination in this type of complexes can be explained through the concept of antisymbiosis[2,3]. A soft donor group energetically prefers a hard donor group when coordinated in a square planar sphere. This explains both the *cis* conformation in **13** and **14** as well as the conformation in **7** and **11**, where *trans* to each soft sulfur atom, a hard donor (O or Cl^-) is found.

In the chelating ring of **13** and **14**, the C-O bond is shortened significantly when compared to free ligands. In addition, the C-S bond is elongated to a larger extent than was observed in the DMSO complexes. This can be interpreted as an increasing double-bond character for the C-O bond and an increasing single-bond character for the C-S bond. The nature of all bonds in the organic chelating unit lies between single and double bonds. The carbon-carbon bonds are of equal length, which confirms a good delocalization of electron density in the chelate. Associated with that is the great stability of this type of complex which explains its occurrence as major product during the synthesis of the platinum-DMSO complexes. The angles of the coordination sphere are greater than 90° for O1-Pt-S1 and O2-Pt-S2 and consequently smaller than 90° for the angles O1-Pt-O2 and S1-Pt-S2. The chelating unit is planar with slightly widened angles, as it was observed for **7** and **11**. Both structures are planar with one tilted alkyl group for **14**. This “reaches” into the next layer of complexes (Figure S3). Still, the molecules are stacked exactly on top of each other.

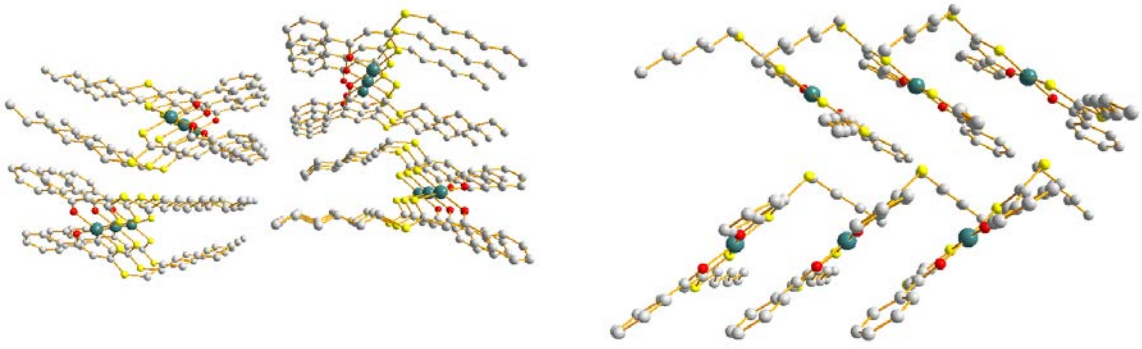

Figure S3. Views of the packing in crystals of **14**. Left, view along the x-axis; right, view along z-axis.

[1] K. Schubert, H. Görls, W. Weigand, *Z. Naturforsch.* **2007**, *62b*, 475–482.
[2] C. K. Jorgensen, *Inorg. Chem.* **1964**, *3*, 1201–1202.
[3] R. G. Pearson, *Inorg. Chem.* **1973**, *12*, 712–713.

Table S3. Crystallographic data for compounds **7**, **11**, **13** and **14.**

Compound		**7**	**11**	**13**	**14**
empirical formula		$C_{12}H_{14}BrClO_2PtS_3$	$C_{13}H_{17}ClO_2PtS_3$	$C_{20}H_{18}O_2PtS_4$	$C_{30}H_{38}O_2PtS_4$
formula mass [g·mol^{-1}]		596.86	531.99	631.67	753.93
collection *T* [°C]		-90(2)	-90(2)	-90(2)	-90(2)
λ (Mo K$_\alpha$) [Å]		0.71073	0.71073	0.71073	0.71073
crystal system		orthorombic	monoclinic	monoclinic	orthorombic
space group (No.)		Pbca (No. 61)	$P2_1/c$ (No.14)	$P2_1/n$ (No.14)	$P2_12_12_1$ (No. 19)
Cell constants	***a* [Å]**	10.3014(3)	7.2779(2)	9.2471(4)	5.6712(1)
	***b* [Å]**	18.1303(5)	38.6448(11)	22.4832(9)	15.4429(3)
	***c* [Å]**	35.8617(12)	11.8038(3)	10.1091(5)	34.9571(6)
	α [°]	90	90	90	90
	β [°]	90	90.262(1)	103.774(3)	90
	γ [°]	90	90	90	90
***V* [Å^3]**		6697.8(3)	3319.82(16)	2041.29(16)	3061.53(10)
Z		16	8	4	4
ρ_{calcd} [g·cm^{-3}]		2.368	2.129	1.997	1.636
μ [cm^{-1}]		112.96	89.88	72.96	48.81
***F*(000)**		4480	2032	1184	1504
crystal dimensions [mm]		0.11×0.09×0.04	0.09×0.08×0.05	0.12×0.08×0.04	0.10×0.09×0.07
2 Θ range [deg]		2.52 < Θ < 72.47	2.80 < Θ < 27.47	2.44 < Θ <27.50	2.33 < Θ < 27.48
index ranges		$-13 \le h \le 13$	$-9 \le h \le 9$	$-12 \le h \le 11$	$-7 \le h \le 6$
		$-23 \le k \le 19$	$-50 \le k \le 49$	$-23 \le k \le 29$	$-19 \le k \le 19$
		$-32 \le l \le 46$	$-15 \le l \le 14$	$-12 \le l \le 13$	$-39 \le l \le 43$
measured reflections		38176	25423	19736	25247
unique reflections		7665	7448	4669	6855
R_{int}		0.1633	0.1051	0.0772	0.0714
data with *I* > 2σ(*I*)		3686	5405	3261	6015
parameters / restraints		367/0	367/0	246/0	337/0
S *		0.877	1.023	1.117	1.005
***R*1 [*I* > 2σ(*I*)]** **		0.0470	0.0467	0.0435	0.0343
***wR*2 [I > 2σ(I)]** ***		0.0570	0.0927	0.0828	0.0516
R1$_{all}$ **		0.1527	0.0799	0.0846	0.0461
***wR*2 [all data, on *F*^{2}]** ***		0.0729	0.1034	0.0949	0.0539
max./min. residual electron density [e·Å^{-3}]		1.190 and -1.751	2.206 and -2.008	1.677 and -1.818	0.560 and -0.975
CCDC-No.		915584	915585	915586	915587

* $S = \left\{\frac{\sum[w(F_o^2 - F_c^2)^2]}{(n-p)}\right\}^{0.5}$ n = no. of reflections, p = no. of parameters

** $R_1 = \frac{\sum||F_o| - |F_c||}{\sum|F_o|}$

*** $wR2 = \left\{\frac{\sum[w(F_o^2 - F_c^2)^2]}{\sum[w(F_o^2)^2]}\right\}^{0.5}$

Behavior in solution

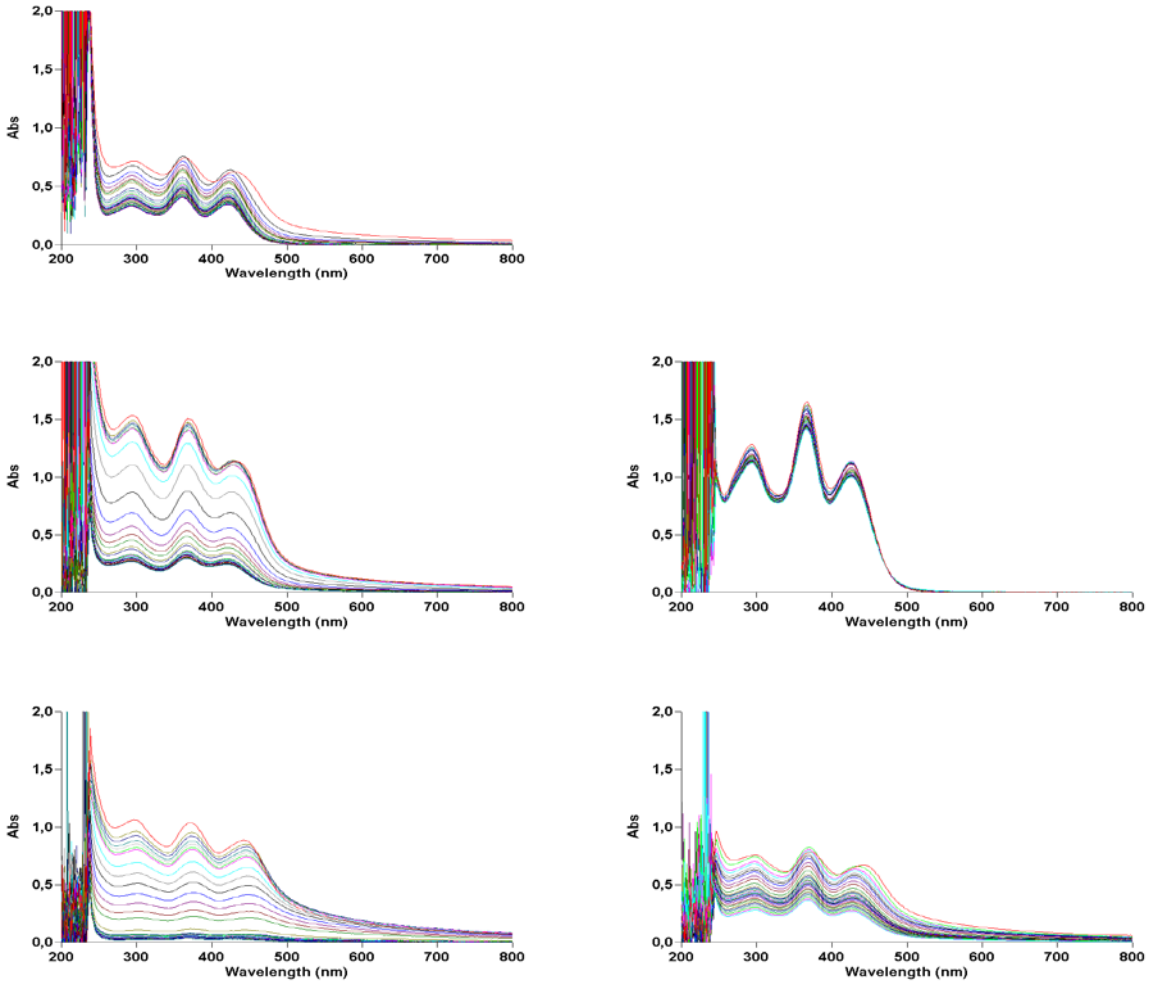

Figure S4. Development of UV-visible absorption spectra of compounds **7** (top), **8** (middle) and **9** (bottom) in 10 % DMSO / 90 % PB (left) and 50 % DMSO / 50 % PB solutions over24 h. Spectra were recorded in 10 min intervals during the first 60 min and hourly afterwards.

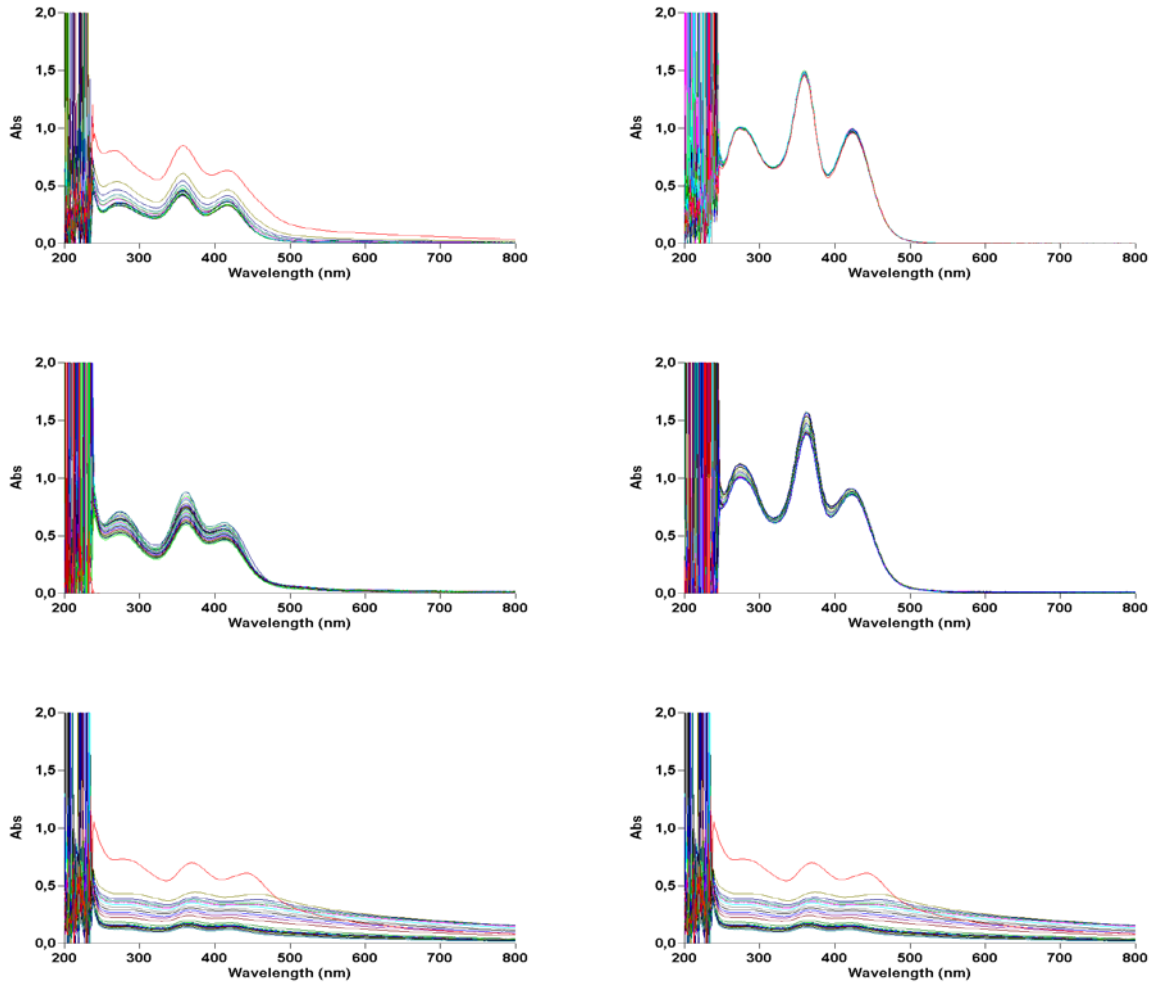

Figure S5. Development of UV-visible absorption spectra of compounds **10** (top), **11** (middle) and **12** (bottom) in 10 % DMSO / 90 % PB (left) and 50 % DMSO / 50 % PB solutions over24 h. Spectra were recorded in 10 min intervals during the first 60 min and hourly afterwards.

Electronic Supplementary Material (ESI) for Dalton Transactions

Biological assay data

Grubbs‘ test for outliers, alpha=5%

$$Z = \frac{|mean - value|}{SD}$$

N	**Critical Z**
3	1.15
4	1.48

4 parameter logistics (4PL)

$$F(x) = \left(\frac{A - D}{1 + \left(\left(\frac{x}{C}\right)^{B}\right)}\right) + D$$

A = minimum asymptote
B = Hill slope
C = inflection point
D = maximum asymptote

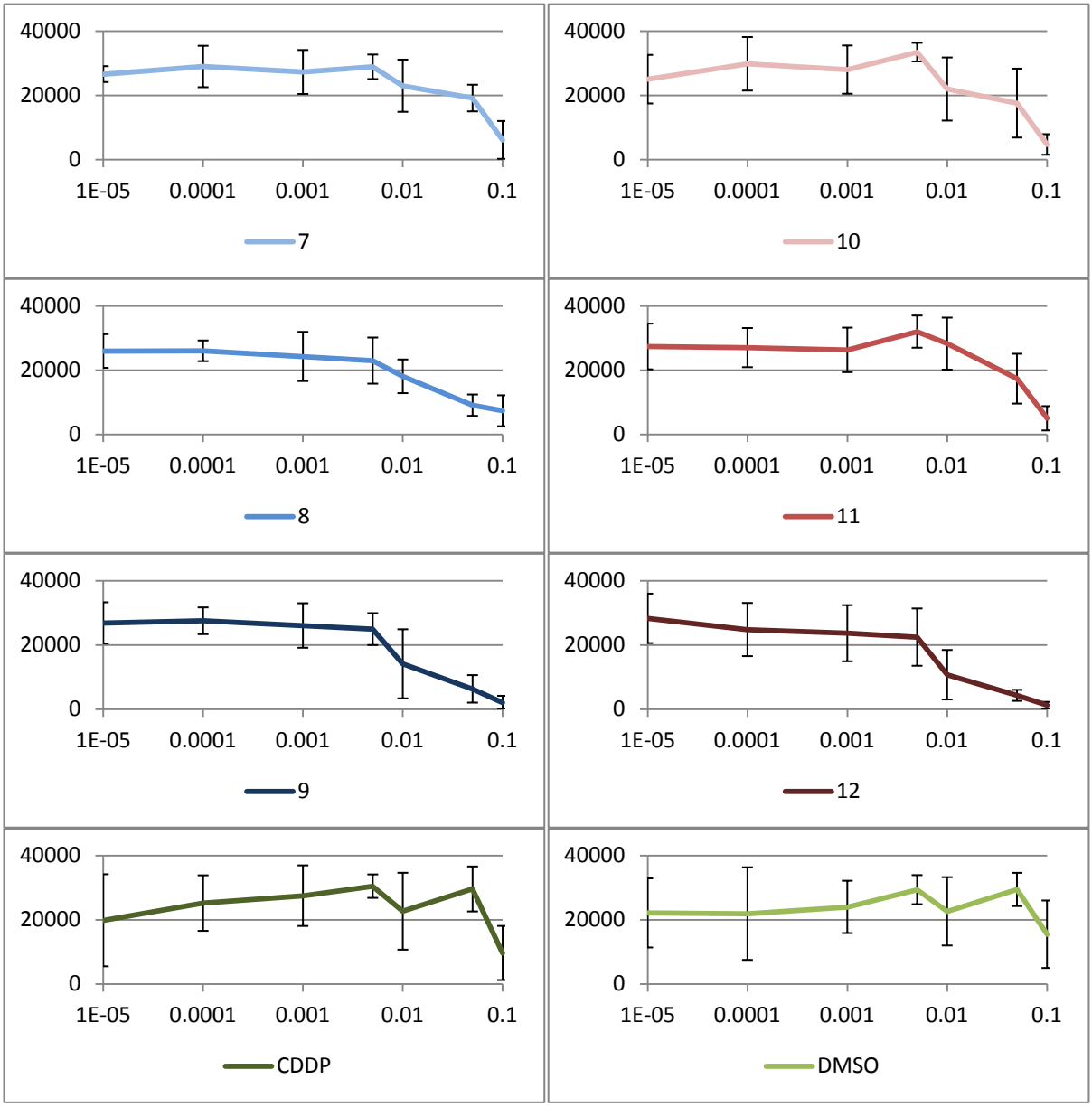

Figure S6. Dose-response curves for sample compounds. X-axis: final drug concentration / mg/mL; Y-axis: fluorescence intensity / a.u. Curves represent the results of 3 independent experiments with quadruplets or triplicate determination of fluorescence intensity for each sample and were corrected by the representative blanks.

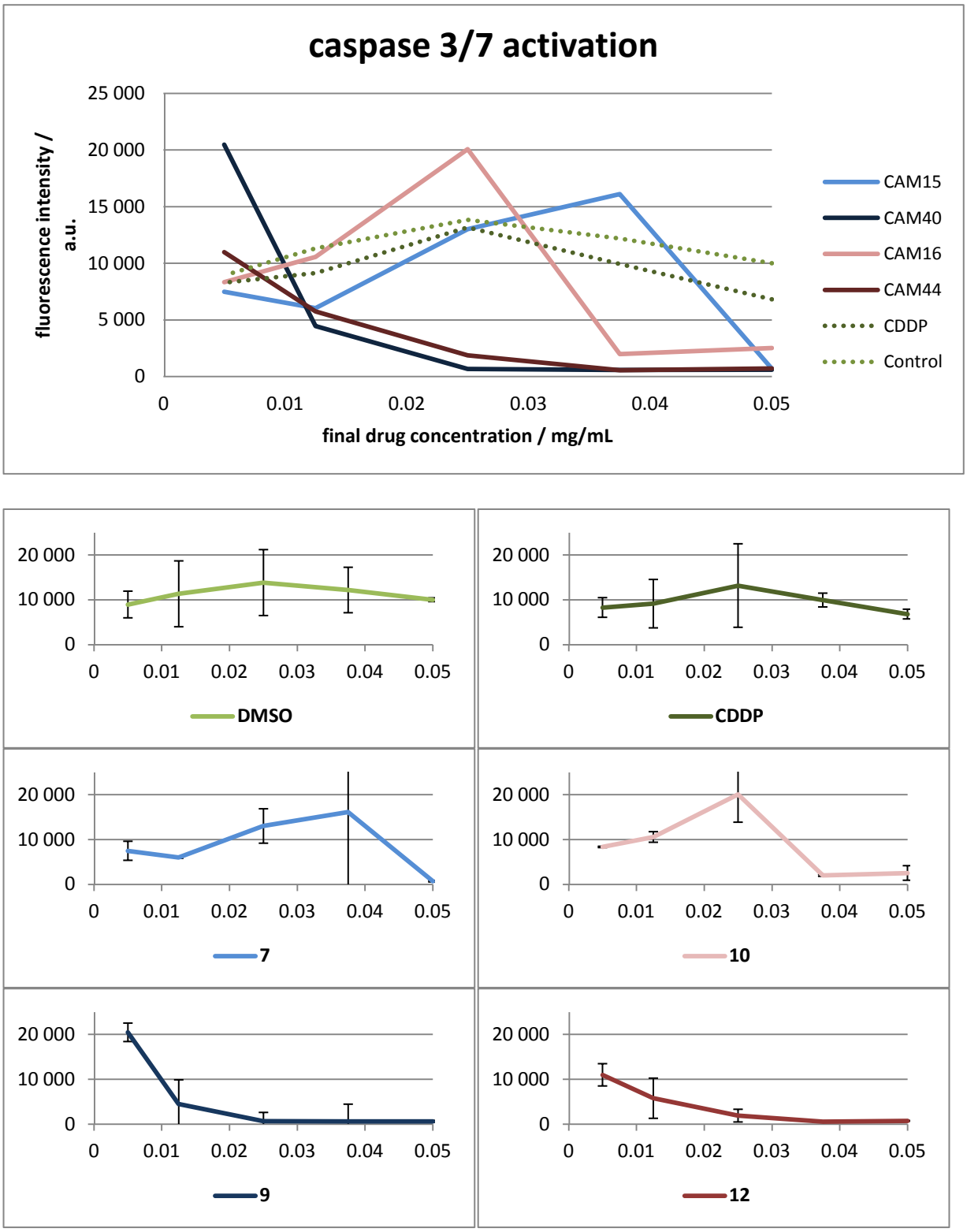

Figure S7. Activation of caspase 3/7 as determined by fluorescence intensity of the rhodamine 110 dye. X-axis: final drug concentration / mg/mL; Y-axis: fluorescence intensity / a.u. Top, overall dose-response curve of all compounds. Below, dose-response curves of single compounds with respective standard deviations.

Mass spectrometric investigations

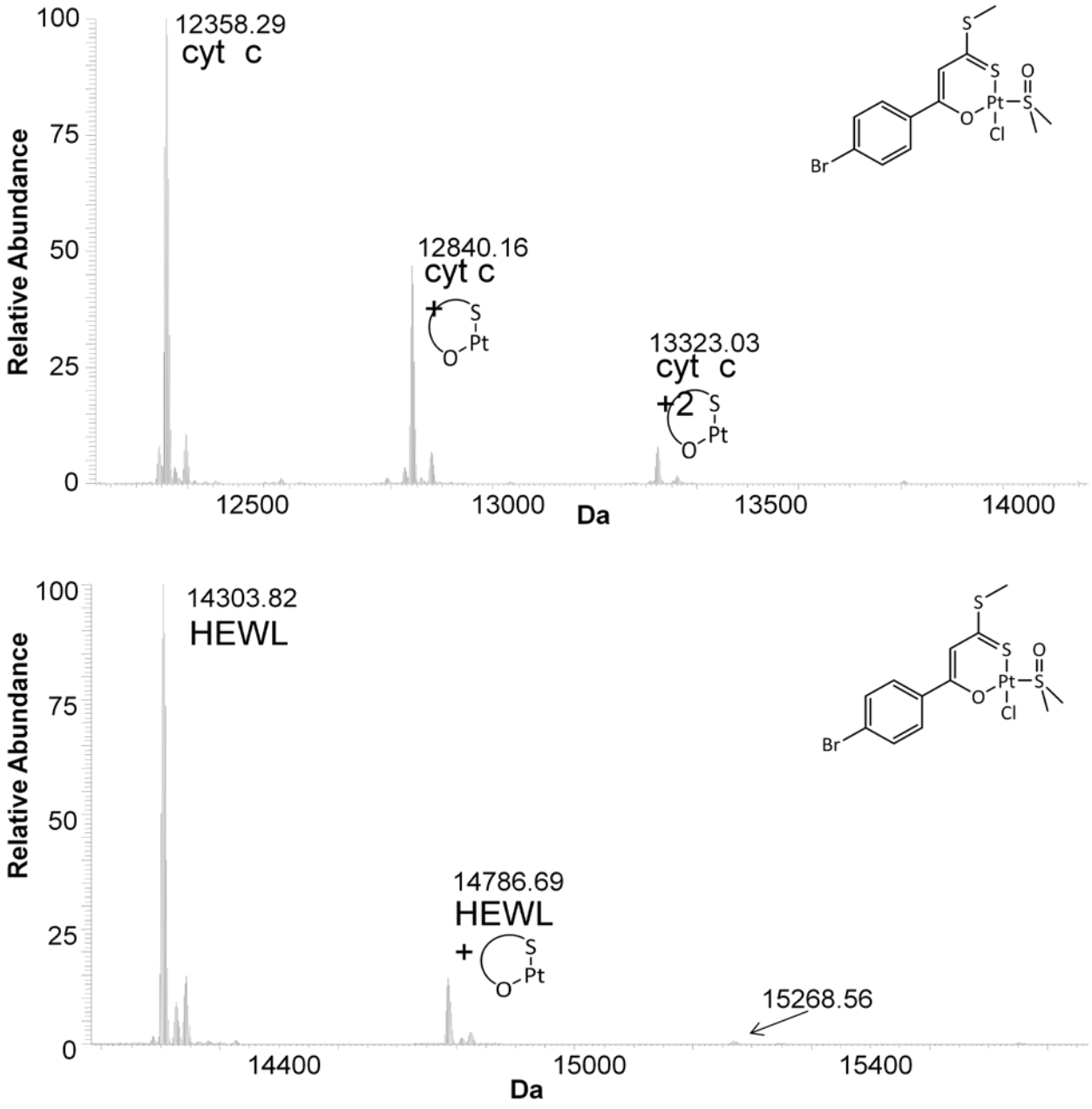

Figure S8. Deconvoluted ESI MS spectra of **7** incubated with cyt c (top) and HEWL (bottom) in a 3:1 metal:protein ratio at 37 °C for 72h.

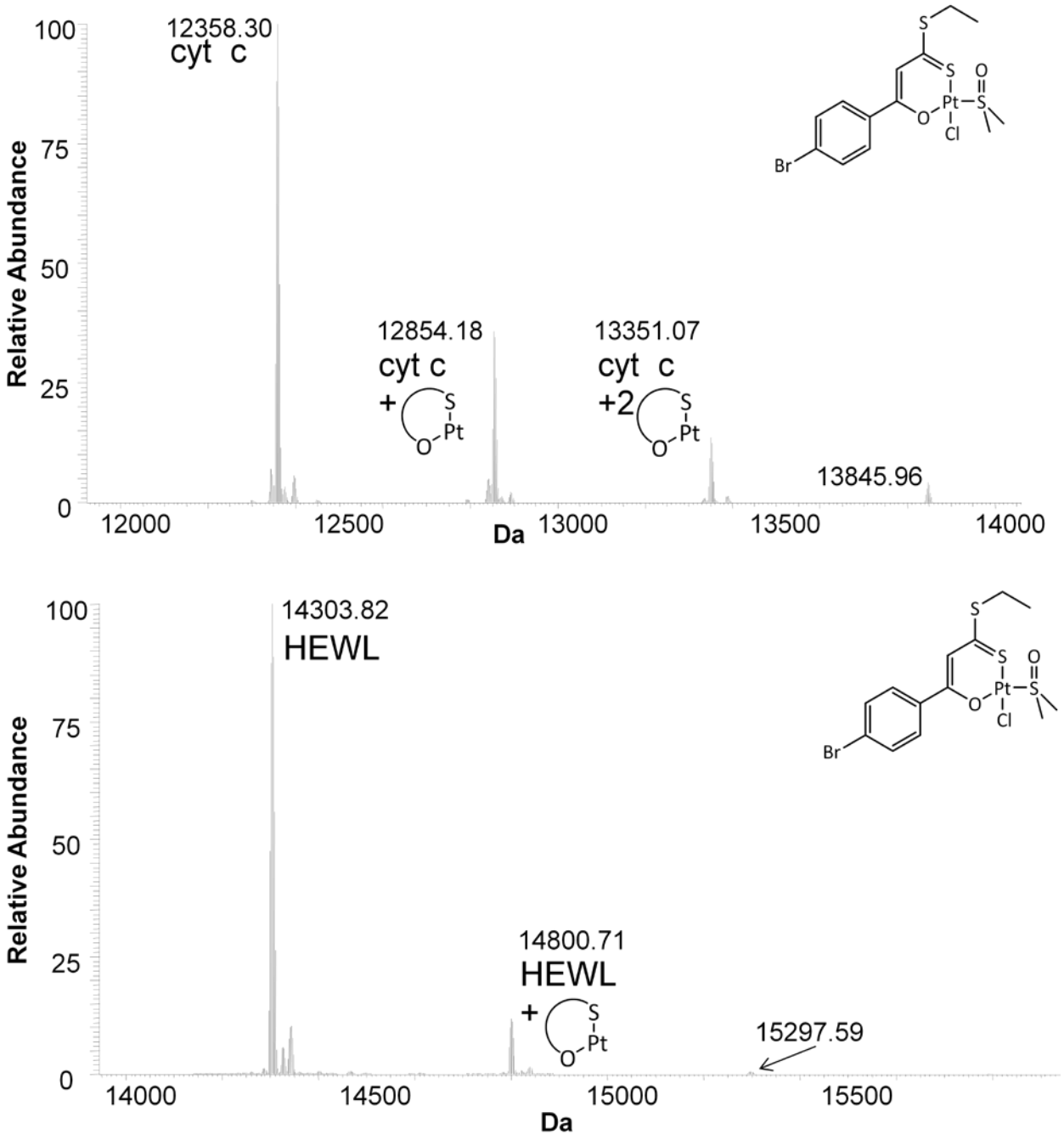

Figure S9. Deconvoluted ESI MS spectra of **8** incubated with cyt c (top) and HEWL (bottom) in a 3:1 metal:protein ratio at 37 °C for 72h.

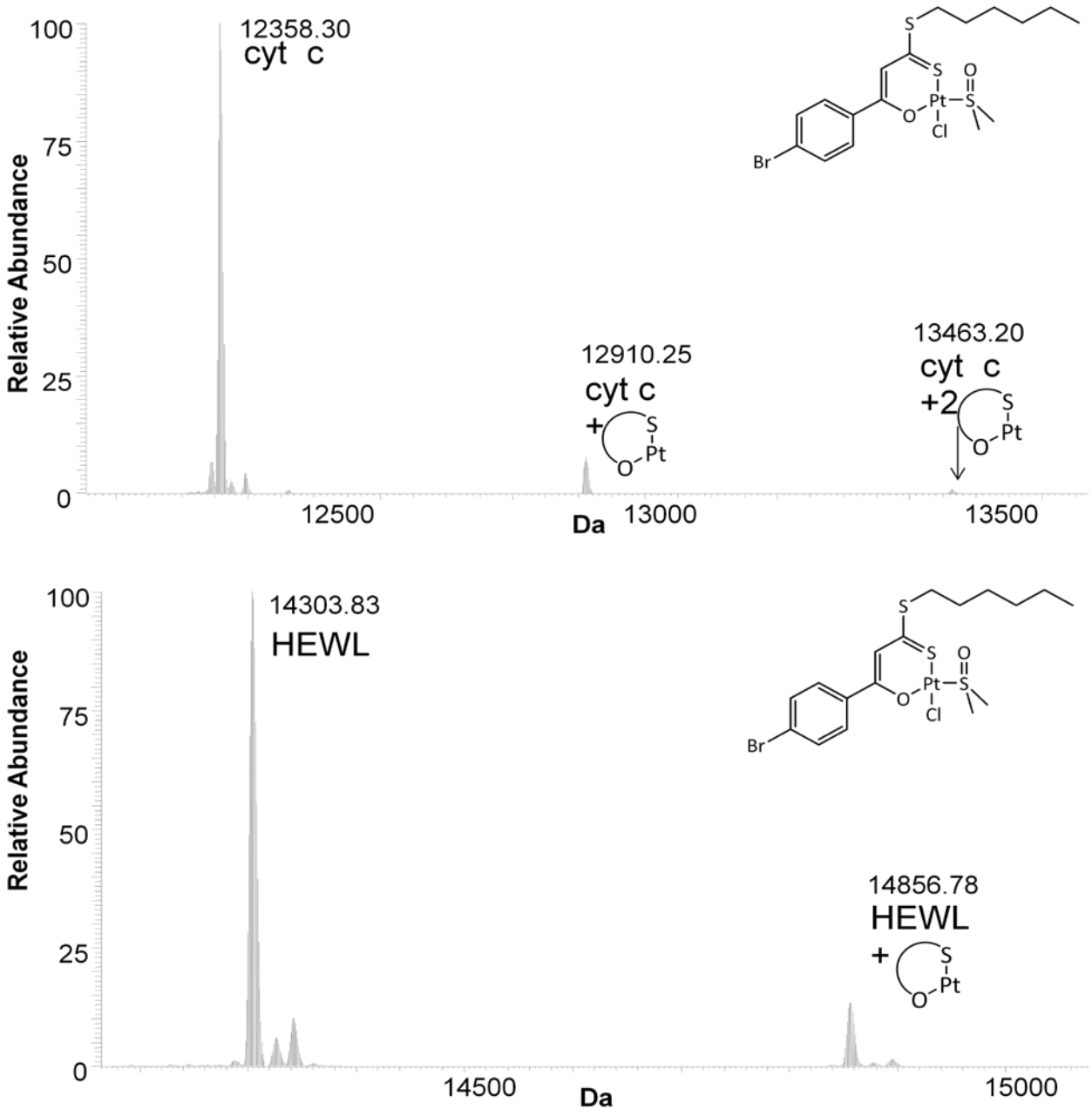

Figure S10. Deconvoluted ESI MS spectra of **9** incubated with cyt c (top) and HEWL (bottom) in a 3:1 metal:protein ratio at 37 °C for 72h.

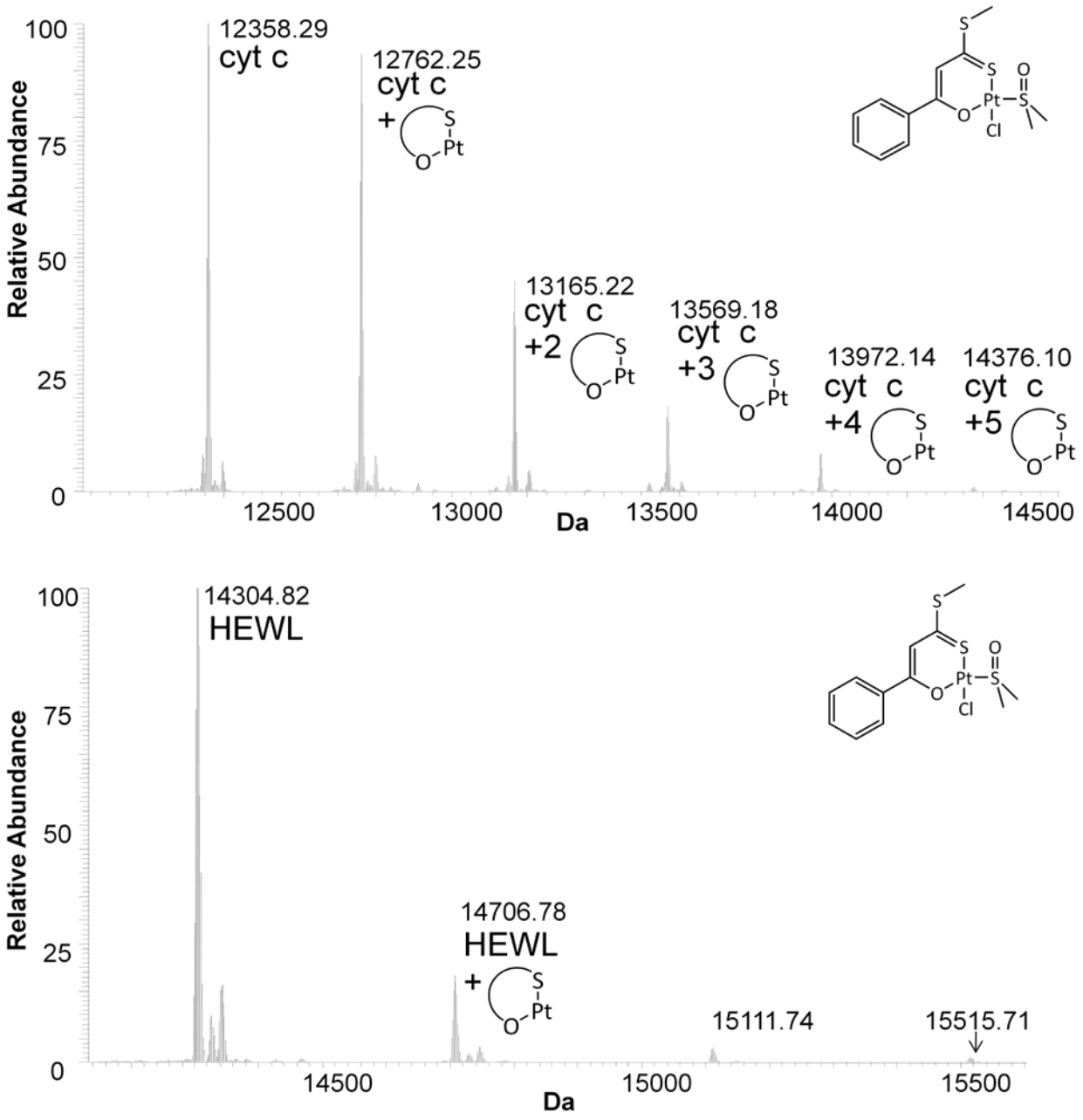

Figure S11. Deconvoluted ESI MS spectra of **10** incubated with cyt c (top) and HEWL (bottom) in a 3:1 metal:protein ratio at 37 °C for 72h.

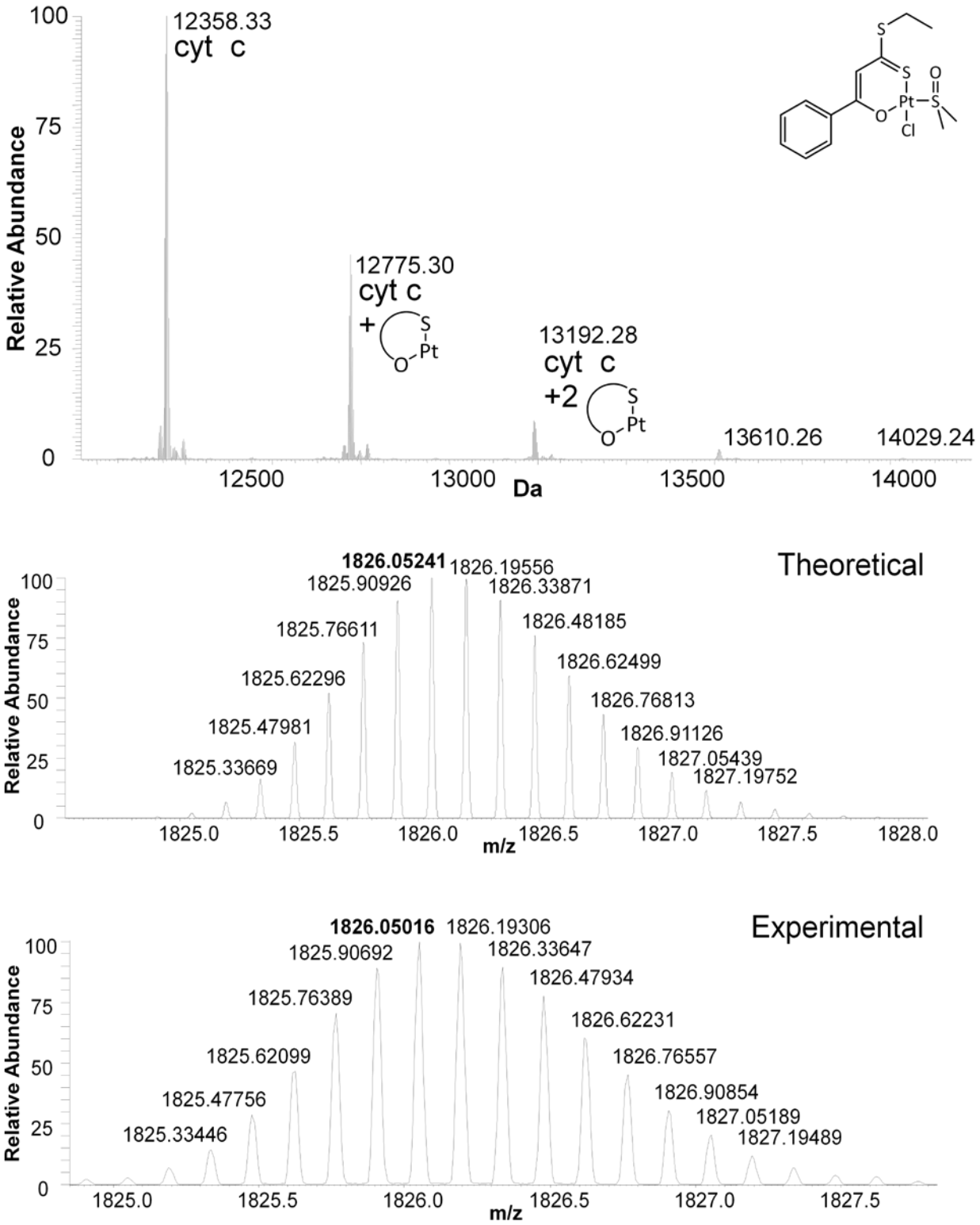

Figure S12. Deconvoluted ESI MS spectrum of **11** incubated with cyt c in a 3:1 metal:protein ratio at 37 °C for 72h (top); theoretical (middle) and experimental (bottom) isotopic pattern for the fragment [CytC(FeIII)$^{+}$ + 5H^{+} + $C_{11}H_{11}O_1S_2Pt_1^{+}$] at charge state +7.

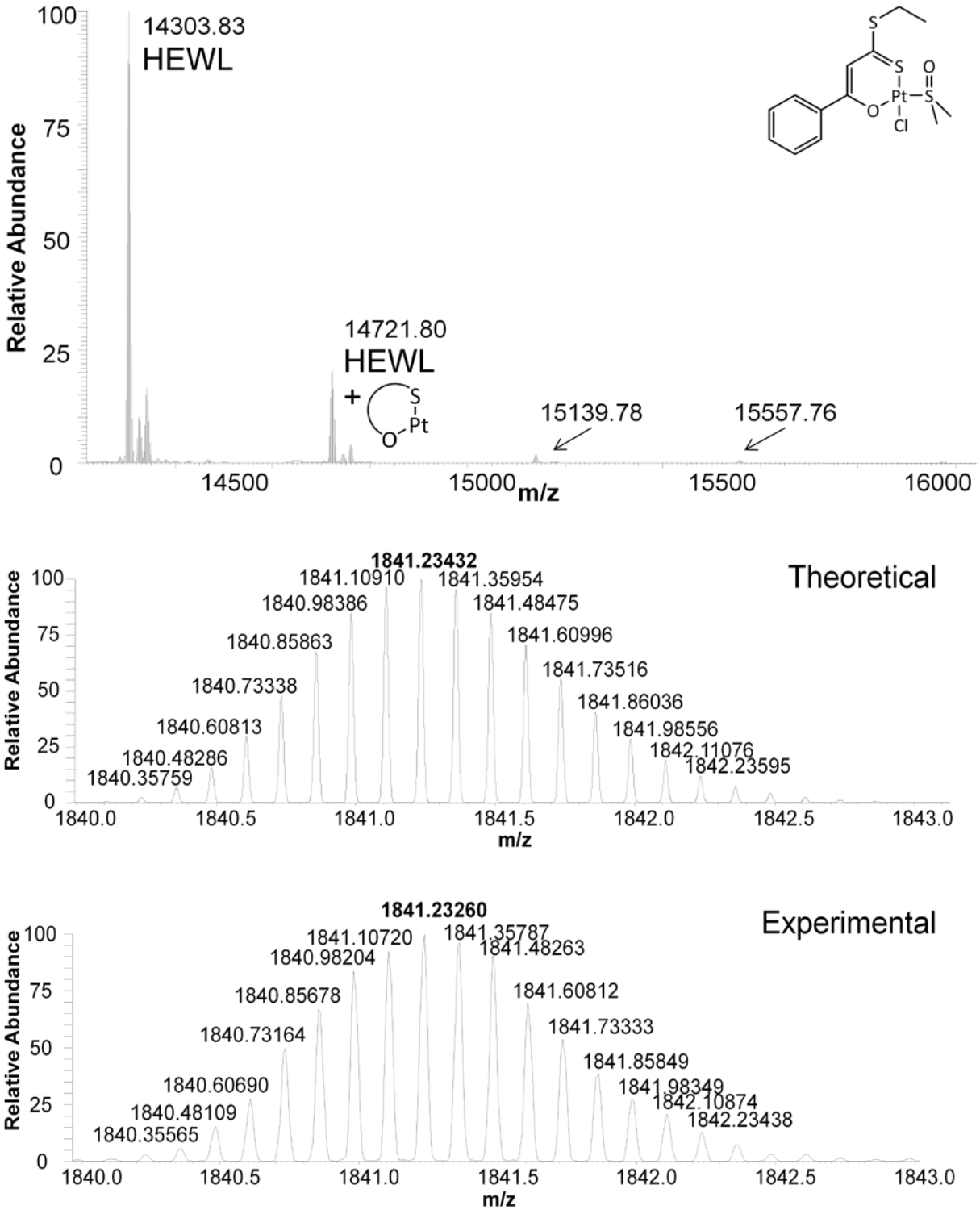

Figure S13. Deconvoluted ESI MS spectrum of **11** incubated with HEWL in a 3:1 metal:protein ratio at 37 °C for 72h (top); theoretical (middle) and experimental (bottom) isotopic pattern for the fragment [Lys + $7H^+$ + $C_{11}H_{11}O_1S_2Pt_1^+$] at charge state +8.

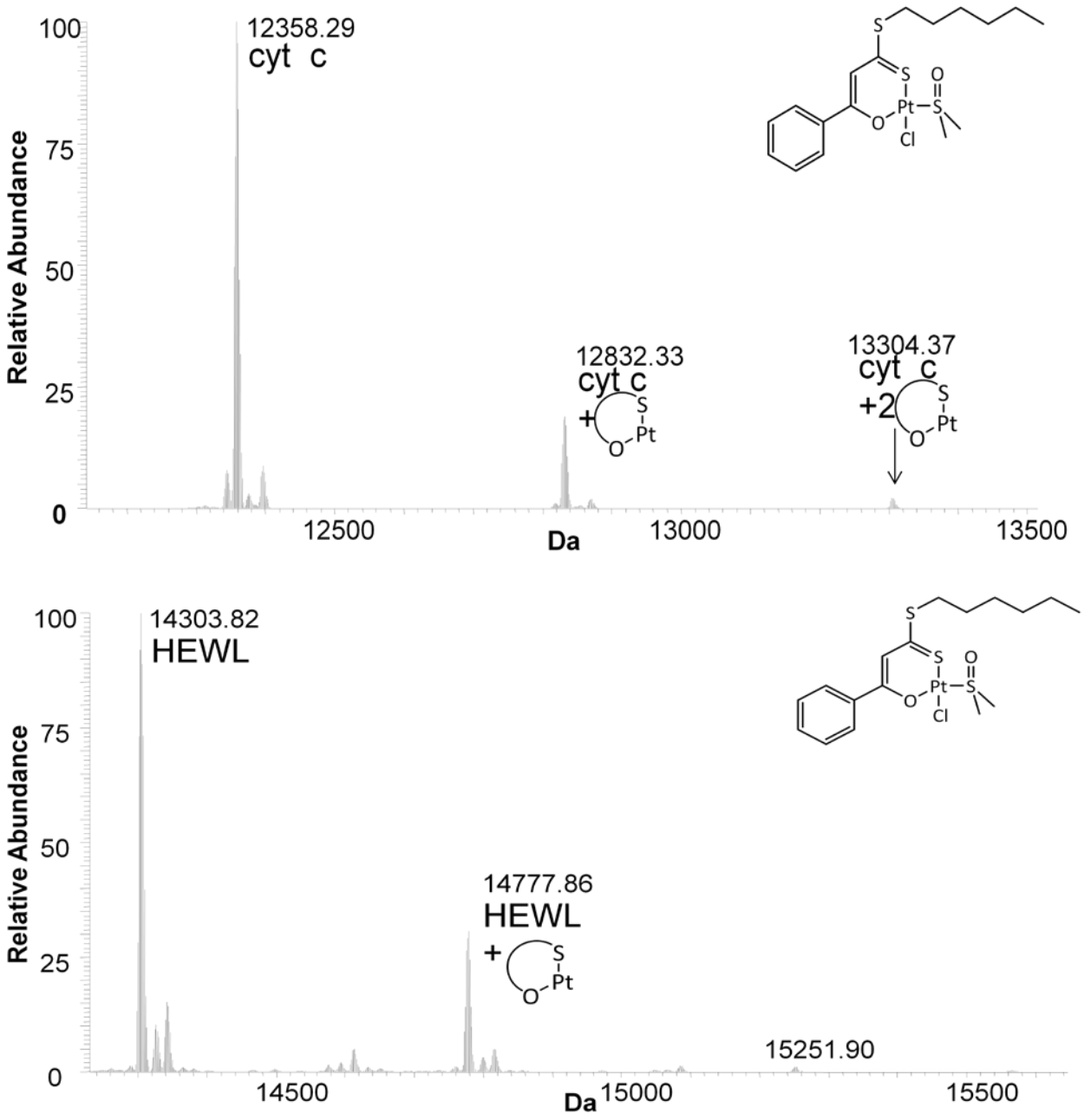

Figure S14. ESI MS spectra of **12** incubated with cyt c (top) and HEWL (bottom) in a 3:1 metal:protein ratio at 37 °C for 72h.